Received 18 July 2023; revised 27 August 2023; accepted 6 September 2023. Date of publication 11 September 2023; date of current version 27 September 2023.

Digital Object Identifier 10.1109/OJCOMS.2023.3313775

Joint Ultrasonic Index Modulation and Splitting Detection for Intra-Body Communications

QIANQIAN WANG [1,2] (Member, IEEE), QUANSHENG GUAN [3] (Senior Member, IEEE), YUANKUN TANG [3] (Graduate Student Member, IEEE), JULIAN CHENG [4] (Fellow, IEEE), FEI JI [3] (Member, IEEE), AND XIANGDONG JIA [1] (Member, IEEE)

[1]College of Computer Science and Engineering, Northwest Normal University, Lanzhou 730070, China
[2]Guangdong Provincial Key Laboratory of Short-Range Wireless Detection and Communication, Guangzhou 510640, China
[3]School of Electronic and Information Engineering, South China University of Technology, Guangzhou 510640, China
[4]School of Engineering, The University of British Columbia, Kelowna, BC V1V 1V7, Canada

CORRESPONDING AUTHOR: Q. GUAN (e-mail: eeqshguan@scut.edu.cn)

This work was supported in part by the National Natural Science Foundation of China under Grant 62301445, Grant 62192712, Grant 62001128, and Grant 62261048; in part by the Natural Science Foundation of Gansu Province under Grant 23JRRA700; and in part by the Open Funding of Guangdong Provincial Key Laboratory of Short-Range Wireless Detection and Communication.

ABSTRACT The reliability of ultrasonic intra-body communication (IBC) is crucial for medical monitoring, diagnosis, and treatment. Recently, ultrasonic splitting receivers that jointly use coherent detection (CD) and non-coherent energy detection (ED) obtain superior bit-error rate (BER) performance compared to a single CD or ED receiver for reliable IBCs. However, this paper demonstrates that existing splitting receivers have performance gains in terms of mutual information and BER in the case of independent channel noises for CD and ED, while no performance gains exist in the case of correlated channel noises. To this end, we propose an ultrasonic index modulation-splitting-maximum ratio combination (UsIM-S-MRC) system. UsIM activates a part of transmission frames whilst S-MRC only processes active frames and treats inactive frames as zero, reducing the average channel noise in all frames. Therefore, the joint-designed UsIM-S-MRC effectively mitigates the impact of channel noise correlation on splitting detection. The theoretical mutual information, BER, and optimal splitting ratio are also derived. Extensive simulations validate the theoretical analysis and reveal that UsIM-S-MRC can attain performance gain in both independent and correlated channel noises, providing a reliable receiver structure for future ultrasonic IBCs.

INDEX TERMS Intra-body communications, ultrasonic communications, ultrasonic index modulation, splitting detection.

I. INTRODUCTION

SEVERAL revolutionary and promising applications like online monitoring and control in the human body have recently emerged for medical treatments. These applications use implantable devices, such as brain-computer interfaces, capsule endoscopes, nanorobots, etc. [1], [2], [3], [4], and require advanced intra-body communication (IBC) technology. The candidate techniques for IBCs can be categorized into radio frequency (RF) communications, optical communications, molecular communications, capacitive coupling, and resonant coupling [1]. However, due to the water-like communication environment and extremely strict safety constraints in the human body, these techniques are limited by transmission distance and power. For instance, the RF wave is severely attenuated in the human body because the water content of the human body is up to 65%, and poses potential risks due to the continuous RF radiation from implants [3]; the transmission distances of optical and molecular IBCs are restricted to a few millimeters [1], [4].

The ultrasonic wave is regarded as a promising medium to enable high data rate IBCs at a communication distance that is greater than tens of centimeters [3], [5]. It is approved by the FDA that the intensity of the ultrasonic wave is about 720 mW/cm^2 in the human body [6], which is much higher

than that of the RF wave (10 mW/cm^2) [7]. In practical applications, the ultrasonic wave has been applied for diagnostic and therapeutic purposes for decades without known side effects. Despite these advantages, ultrasonic IBCs face the following challenges. The ubiquitous tissues and organs can cause reflections and refraction of the transmitted signals, resulting in severe multipath effects. Furthermore, due to the fact that organs are vulnerable and battery replacement in the human body is costly, IBC has strict constraints on transmission power, implant size, and energy consumption.

Motivated by the fact that medical ultrasonic applications usually adopt ultrasonic pulses [8], the ultrasonic pulse with high resolution and low duty cycle provides an effective solution to the aforementioned challenges [9]. Existing ultrasonic pulse-based IBC systems mainly focus on improving data rates, e.g., time-hopping ultrasonic wideband (TH-UsWB) [9], direct-sequence UsWB (DS-UsWB) [10], and ultrasonic index modulation (UsIM) [11]. In addition to data rate, reception reliability is also critical for medically targeted ultrasonic IBCs. Recently, a splitting receiver has been extensively investigated for providing better performance compared with a single coherent detection (CD) or non-coherent energy detection (ED) receiver [12], [13], [14]. The fundamental is that the joint use of CD and ED can simultaneously detect amplitude and phase, which are detected by CD, as well as energy, which is detected by ED, and thus more signal attributes can be employed to achieve reliable reception [14]. Specifically, the ultrasonic splitting receiver splits the received signal into two streams, which are processed by CD and ED respectively, and then the CD and ED signals are combined for information decoding for M-ary pulse position modulation (M-PPM)-based IBCs [14]. The channel noises in CD and ED are generally ignored [12] or assumed to be independent [14]. However, when the CD and ED signals in the ultrasonic splitting receiver are split from the same received signal, the channel noises in CD and ED come from the same noise, which means that they are completely correlated. In this case, it is desirable to address the question of whether the performance gain still exists and how to achieve the performance gain under correlated channel noises.

This paper investigates the impact of channel noise correlation on ultrasonic splitting receivers. In practice, two signal splitters, namely time switching (TS) and power splitting (PS), are generally used to split the received signal [15], [16]. TS periodically switches between CD and ED branches, leading to independent channel noises in CD and ED, whereas PS splits the received signal into two streams with different power levels, resulting in completely correlated channel noises in CD and ED. We investigate the performance of splitting receivers in both TS and PS cases. Our results demonstrate that the existing ultrasonic splitting receiver [14] has performance gain when using TS, but all power should be allocated to CD to obtain optimal performance when using PS. Consequently, although the existing ultrasonic splitting receiver detects multiple attributes of the received signal, the optimal detection is the traditional CD when using the PS splitter.

This paper further investigates how to attain performance gain for the receiver using the PS splitter. The core idea is to jointly design the transmitter and receiver to mitigate the impact of channel noise correlation on splitting detection. We propose a joint-designed UsIM-splitting-maximum ratio combination (UsIM-S-MRC) system consisting of a UsIM transmitter and an S-MRC receiver. The advantages of the proposed UsIM-S-MRC system come from two aspects. First, UsIM transmits information bits by ultrasonic pulses in the active frames and the index of the active frames [11], [17], [18], and hence uses a part of transmission frames. Second, to detect the active frames, S-MRC performs a correlation operation on the template signal[1] and the received signal to achieve CD and conducts the square operation on the estimated active frames to achieve ED. Therefore, benefiting from UsIM and S-MRC, the channel noise component exists only in the active frames and thus the average channel noise within all frames can be mitigated.

In a preliminary work, we proposed a splitting detection-joint simplified MRC (SD-JsMRC) receiver, which uses TS to achieve independent channel noises for CD and ED [19], and provided bit-error rate (BER) derivation for the UsIM system employing only one active frame and binary PPM. In this paper, we propose a generalized S-MRC receiver in which the signal can be detected by different signal splitters (including TS and PS) and then demodulated by MRC. Taking practical scenarios into account that the template signal may not be perfectly synchronized with the received signal in CD, the performance of the receiver with and without synchronization error is investigated for a generalized UsIM that has multiple active frames and performs M-PPM. The contributions of this paper are summarized as follows:

- We investigate the impact of channel noise correlation on ultrasonic splitting receivers, using two signal splitters, including TS and PS, for IBCs. We find that the existing ultrasonic splitting receiver has no performance gain when the channel noises in CD and ED are completely correlated.
- We propose a UsIM-S-MRC system to mitigate the impact of channel noise correlation on splitting detection, attaining performance gain for IBC systems in terms of mutual information and BER in both cases of independent and correlated channel noises.
- Considering the synchronization error, we derive the theoretical mutual information, BER, and optimal splitting ratio of UsIM-S-MRC using TS and PS over intra-body fading channels, since the timing synchronization of the template signal and the received signal in CD is critical to the receiver performance.

Extensive Monte Carlo simulations validate the theoretical analysis and reveal that UsIM-S-MRC can achieve the

1. The template signal consists of pulses in the estimated active frames and zeros in inactive frames [11].

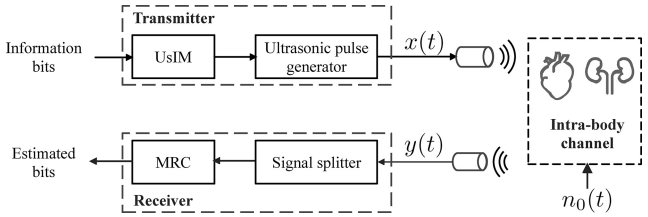

FIGURE 1. System structure of UsIM-S-MRC for ultrasonic IBCs.

lowest BER for UsIM systems with synchronization errors, providing a robust and superior reception scheme for IBCs.

The remainder of this paper is organized as follows: In Section II, the UsIM-S-MRC system is proposed for IBCs. Section III analyzes the channel noise correlation in UsIM-S-MRC and system performance in terms of BER, optimal splitting ratio, mutual information, and throughput. The simulation results are explored in Section IV, and conclusions are drawn in Section V.

Notation: Upper case boldface letters and lower case boldface letters denote matrices and column vectors, respectively. The probability density function (PDF) and the probability of an event are denoted by $f(\cdot)$ and $\Pr(\cdot)$, respectively. $\mathbb{C}(\cdot,\cdot)$ denotes the binomial coefficient. $\lfloor\cdot\rfloor$ denotes the floor function. $\delta(\cdot)$ and $\Gamma(\cdot)$ denote the Dirac delta function and the gamma function, respectively. $\mathrm{I}(\cdot,\cdot)$ and $\mathrm{H}(\cdot)$ denote the mutual information and the entropy, respectively. $\mathbb{E}[\,\cdot\,]$ denotes expectation, and $\mathbb{E}_h[\cdot]$ denotes the expectation with respect to h. $Q(\cdot)$ denotes the Gaussian Q-function. $I_0(\cdot)$ denotes the first kind modified Bessel function of order zero.

II. SYSTEM DESIGN OF USIM-S-MRC

The UsIM-S-MRC system contains three main parts: transmitter, channel, and receiver, as shown in Fig. 1. The transmitter employs UsIM to modulate the information bits and generates ultrasonic pulses that propagate via the intra-body channel. The signal is detected by the signal splitter and demodulated by MRC. Note that due to the fundamental differences between ultrasonic pulses and RF waves, the ultrasonic splitting receiver does not require two circuits for the CD and ED receivers to generate separate CD and ED signals as independent decision variables and it performs diversity combination of the CD and ED signals in one circuit.[2] The detailed signal processing in each block of UsIM-S-MRC is illustrated as follows.

A. TRANSMITTED SIGNAL OF USIM

Suppose the transmitted signal is organized by frames. One transmission block is transmitted by L frames, and one frame consists of M chips to implement M-PPM to transmit the modulation bits. To enable both CD and ED in the receiver, PPM is adopted in the transmitter, and thus we use "PPM bits" in this paper to specifically represent "modulation bits".

2. It is demonstrated that the ultrasonic splitting receiver is superior to the RF-based splitting receivers in terms of lower complexity and lower BER with imperfect channel estimation [12], [13], [14].

TABLE 1. Summary of frequently used symbols.

Symbol	Description
p	The number of information bits per block
p_1	The number of PPM bits per block
p_2	The number of index bits per block
L	The number of frames per block
M	The number of chips per frame
K	The number of active frames per block
Ω_j	The index of the j-th active frame combination
Ω_j^i	The position of the i-th active frame of Ω_j
c_l	The index of the l-th chip combination used to transmit the K ultrasonic pulses
c_l^i	The position of the i-th chip of c_l

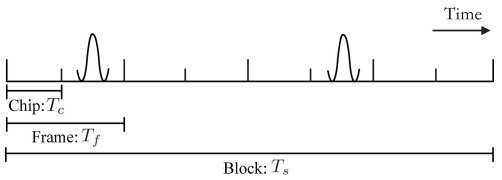

FIGURE 2. A waveform example of UsIM with 2-PPM for a bit block "1101", where the PPM bits are "11" and the index bits are "01". The corresponding chip index and frame index are respectively c_4 and Ω_2 in Tab. 2.

TABLE 2. Example of indices and information bits mapping of UsIM for $p_1 = 2$, $p_2 = 2$, $L = 4$, $M = 2$, and $K = 2$.

Index bits	frame index	Modulation bits	chip index
[0 0]	$\Omega_1 = \{0, 1\}$	[0 0]	$c_1 = \{0\ 0\}$
[0 1]	$\Omega_2 = \{0, 2\}$	[0 1]	$c_2 = \{0\ 1\}$
[1 0]	$\Omega_3 = \{0, 3\}$	[1 0]	$c_3 = \{1\ 0\}$
[1 1]	$\Omega_4 = \{1, 2\}$	[1 1]	$c_4 = \{1\ 1\}$

The duration of one block, one frame, and one chip are T_s, T_f, and T_c, respectively. Therefore, we have $T_s = LT_f$ and $T_f = MT_c$. UsIM uses the index of the active frames to carry additional information bits. The information bits are divided into blocks with p bits, including p_1 PPM bits and p_2 index bits. Hence, we have $p = p_1 + p_2$.

Assuming that K of L frames are activated to transmit PPM bits, there are $\mathbb{C}(L, K)$ indices of active frame combination to convey p_2 index bits, and $p_2 = \lfloor \log_2 \mathbb{C}(L, K) \rfloor$. The p_1 PPM bits are transmitted by K ultrasonic pulses and $p_1 = K \log_2 M$. The frequently used symbols are listed in Tab. 1, where $\Omega_j^i = 0, \ldots, L-1$, $c_l^i = 0, \ldots, M-1$, $j = 1, \ldots, 2^{p_2}$, $l = 1, \ldots, M^K$, and $i = 1, \ldots, K$. Take $p_1 = 2$, $p_2 = 2$, $L = 4$, $M = 2$, and $K = 2$ as an example, the information bits mapping is shown in Tab. 2. Moreover, a transmission waveform example of UsIM for a bit block "1101" is depicted in Fig. 2, which corresponds to c_4 and Ω_2 in Tab. 2.

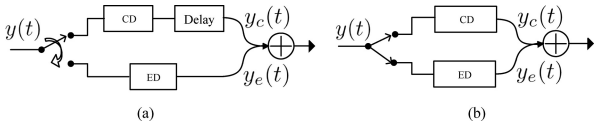

FIGURE 3. Structures of (a) TS and (b) PS.

The output of UsIM is a $1 \times ML$ vector and expressed as

$$\mathbf{x} = \left[x_{0,0}, \ldots, x_{0,M-1}, \ldots, x_{L-1,0}, \ldots, x_{L-1,M-1}\right], \quad (1)$$

where the element $x_{k,m} \in \{0, 1\}$, $k = 0, 1, \ldots, L-1$ and $m = 0, 1, \ldots, M-1$. Suppose the index bits are conveyed by Ω_j and the PPM bits are conveyed by c_l. The vector of UsIM can be expressed as $\mathbf{x}_{\Omega_j, c_l}$, where the active element $x_{\Omega_j^i, c_l^i} = 1$, and other inactive elements have values of zeros. Hence, the transmitted signal waveform is given by

$$x(t) = \sum_{k=-\infty}^{\infty} \sum_{i=1}^{K} \sqrt{E_p} p\left(t - kT_s - \Omega_j^i T_f - c_l^i T_c\right), \quad (2)$$

where $p(t)$ is the transmitted monocycle waveform of one pulse with normalized energy of $\int_{-\infty}^{\infty} p^2(t)dt = 1$, the pulse width[3] is T_p, and E_p is the energy of one transmitted pulse. For brevity, this paper analyzes the first information block, and other information blocks can be analyzed similarly. We can rewrite (2) as

$$x(t) = \sum_{i=1}^{K} \sqrt{E_p} p\left(t - \Omega_j^i T_f - c_l^i T_c\right). \quad (3)$$

B. SIGNAL SPLITTING

Figure 3 depicts two different signal splitters, including TS and PS.[4] Specifically, TS periodically switches between the CD and ED branches, whereas PS splits the received signal into two streams with different power levels. The signal splitter first splits the received signal into two streams detected by CD and ED respectively. Then, the detected CD and ED signals are combined for demodulation in MRC. It is worth noting that whether the signal is split in the time domain with TS or in the power domain with PS, the role of these power splitters is to split the power of the received signal. Therefore, to be consistent with the term "power splitter", we use "power splitting ratio" for both TS and PS cases in the sequel.

The received signal $y(t)$ is expressed as

$$y(t) = hx(t) + n_0(t), \quad (4)$$

where h is the channel coefficient, which is assumed to be invariant within one frame duration, and $n_0(t)$ is zero-mean additive white Gaussian noise with power spectral density $N_0/2$. Since the propagation of ultrasonic waves in tissues is affected by attenuation and small-scale fading, the channel coefficient is given by $h = H\vartheta$, where $H = \sqrt{e^{-\zeta d}}$ represents the attenuation coefficient, and d is the transmission distance [3]. The amplitude attenuation coefficient ζ (in $[\text{np} \cdot \text{cm}^{-1}]$) is a function of the central frequency of a channel as $\zeta = af^b$, where a and b are the attenuation parameters that characterize the tissue [3]. The parameter ϑ denotes the fading coefficient of intra-body channels. According to the experimental results from a kidney phantom, the distribution of ϑ follows a generalized Nakagami distribution [7], [20], which is given by

$$f(\vartheta) = \frac{2z\alpha^{\alpha} \vartheta^{2z\alpha-1}}{\Gamma(\alpha)\beta^{\alpha}} e^{-\frac{\alpha}{\beta}\vartheta^{2z}}, \quad (5)$$

where α, β, and z are the shaping, spreading, and generalization parameters, respectively.

The signal in the CD branch is multiplied by the template signal $m(t)$, i.e., [21],

$$m(t) = \sum_{i=0}^{L-1} \sum_{m=0}^{M-1} \sqrt{E_p} p\left(t - iT_f - mT_c\right). \quad (6)$$

The $m(t)$ means that each chip has an ultrasonic pulse with energy E_p. Then, the CD signal is given by

$$y_c(t) = \sqrt{\rho} y(t + \tau_e) m(t), \quad (7)$$

where ρ is the power splitting ratio and τ_e is the timing synchronization error in the receiver.[5]

The ED branch processes the received signal by the square operation to generate the ED signal, which is given by

$$y_e(t) = \left(\sqrt{1-\rho} y(t + \tau_e)\right)^2. \quad (8)$$

The output of the signal splitter, which combines the CD and ED signals, is given by

$$y_s(t) = y_c(t) + y_e(t). \quad (9)$$

Note that RF-based splitting receivers consider the receiver noises [12], [13], including the conversion noise due to the conversion from the RF band to baseband in the CD receiver, and the rectifier noise due to the conversion of the RF signal to a direct current (DC) signal in the power detection receiver. The aforementioned receiver noises do not exist in ultrasonic splitting receivers, since ultrasonic pulses are baseband signals.

C. DECISION OF MRC

To demodulate the information bits, the MRC first demaps the index bits, i.e., the inverse operation of the mapping process from index bits to frame index. Then, the PPM bits

3. The relationship between T_c and T_p should be $T_c \gg T_p$ to avoid inter-chip-interference and inter-frame-interference caused by the multipath effect in the human body [10], [11].

4. Note that different from the simultaneous wireless information and power transfer [15], [16], the split signal streams of CD and ED from TS/PS in this paper are used for information decoding.

5. A promising system structure for intra-body networks consists of multiple implanted devices and a central coordinator/sink that can perform time synchronization by sending out regular beacons or other advanced methods [11].

are demodulated within the demapped frames. Specifically, the received pulses are converted into discrete signals by integrating $y_s(t)$ within each chip duration. We obtain the vector of the received signal as

$$\mathbf{y} = \left[y_{0,0}, \ldots, y_{0,M-1}, \ldots, y_{L-1,0}, \ldots, y_{L-1,M-1}\right], \quad (10)$$

where the elements $y_{k,m}$ ($k = 0, 1, \ldots, L-1$, and $m = 0, 1, \ldots, M-1$) consisting of the CD and ED signals are given by

$$y_{k,m} = \int_{\tau_{k,m}}^{\tau_{k,m+1}} \left[y_c(t) + y_e(t)\right] dt = y_{c_{k,m}} + y_{e_{k,m}}, \quad (11)$$

herein $\tau_{k,m}$ represents the start time of the m-th chip within the k-th frame.

The sum of integrals within one block is denoted by y_{Ω_j}, corresponding to one of the 2^{p_2} possible indices, i.e.,

$$y_{\Omega_j} = \sum_{i=1}^{K} \int_{\tau_{\Omega_j^i,0}}^{\tau_{\Omega_j^i,M}} \left[y_c(t) + y_e(t)\right] dt, \quad (12)$$

where $j = 1, \ldots, 2^{p_2}$. The decision criterion follows [11][6]

$$\Omega_{\hat{j}} = \underset{j \in \{1,\ldots,2^{p_2}\}}{\arg\max} \left\{y_{\Omega_j}\right\}. \quad (13)$$

The index bits, accordingly, can be recovered from $\Omega_{\hat{j}}$. Then, the p_1 PPM bits can be demodulated according to

$$\hat{c}_l = \underset{l \in \{1,\ldots,M^K\}}{\arg\max} \left\{y_{\Omega_{\hat{j}}, c_l}\right\}. \quad (14)$$

D. SYSTEM COMPLEXITY

Let the computational complexity of a system be represented by the total number of multiplications performed per information block. For p bits, including p_1 PPM bits and p_2 index bits, the computational complexity of S-MRC is $\mathcal{O}(2)$ in the detection stage and is $\mathcal{O}(2^{p_2} + KM)$ in the MRC stage. Therefore, the complexity of S-MRC is given by

$$\mathcal{O}_{\text{S-MRC}} = 2 + 2^{p_2} + KM. \quad (15)$$

The complexity of CD-based maximum likelihood (C-ML), C-MRC for UsIM [11], and splitting-detection joint-decision (SDJD) for 2^p-PPM [14] are respectively given by

$$\begin{aligned} \mathcal{O}_{\text{C-ML}} &= 1 + 2^{p_2} M^K, \\ \mathcal{O}_{\text{C-MRC}} &= 1 + 2^{p_2} + KM, \\ \mathcal{O}_{\text{SDJD}} &= 2 + 2^p. \end{aligned} \quad (16)$$

Remark 1: It is worth noting that $M^K = 2^{p_1}$ and thus $2^{p_2} M^K = 2^p$. It can be derived that the complexity of all receivers for UsIM is lower than that of SDJD, since SDJD uses CD and ED to detect the received signal and compares all possible transmitted signals. This reveals an important advantage of UsIM over PPM, i.e., UsIM can transmit the same number of bits as PPM with much lower complexity, which is significant for size- and energy-constrained IBCs.

6. The MRC in [11] requires additional absolute value operations on y_{Ω_j}. Thus, the MRC structure in this paper is simplified.

III. CHANNEL NOISE CORRELATION AND PERFORMANCE ANALYSIS

In this section, we first detail the signal models and investigate channel noise correlation. Then, we derive and analyze the BER, optimal splitting ratio, mutual information, and throughput in both TS and PS cases. Without loss of generality, in the following analysis, let the index bits be conveyed by Ω_j and the PPM bits be conveyed by c_l.

A. RECEIVED SIGNAL MODELS

The detected CD signal in the c_l^i chip of the Ω_j^i frame, where $i = 1, \ldots, K$, is given by

$$\begin{aligned} y_{c_{\Omega_j^i, c_l^i}} &= \int_{\tau_{\Omega_j^i, c_l^i}}^{\tau_{\Omega_j^i, c_l^i + 1}} y_c(t) dt \\ &= hR_0(\tau_e)\sqrt{\rho} E_p + \sqrt{\rho E_p} n_{c_{\Omega_j^i, c_l^i}}, \end{aligned} \quad (17)$$

where $R_0(\tau_e)$ is the synchronization coefficient of CD and is a function of the timing synchronization error τ_e, i.e.,

$$\begin{aligned} R_0(\tau_e) = \int_{\tau_{\Omega_j^i, c_l^i}}^{\tau_{\Omega_j^i, c_l^i + 1}} & p\left(t - \Omega_j^i T_f - c_l^i T_c\right) \\ & \times p\left(t - \Omega_j^i T_f - c_l^i T_c + \tau_e\right) dt. \end{aligned} \quad (18)$$

The detected ED signal in the c_l^i chip of the Ω_j^i frame is

$$\begin{aligned} y_{e_{\Omega_j^i, c_l^i}} &= \int_{\tau_{\Omega_j^i, c_l^i}}^{\tau_{\Omega_j^i, c_l^i + 1}} y_e(t) dt \\ &= (1-\rho)\left(h^2 R_1(\tau_e) E_p + 2h\sqrt{E_p R_1(\tau_e)} n_{e_{\Omega_j^i, c_l^i}} + \eta_{e_{\Omega_j^i, c_l^i}}\right), \end{aligned} \quad (19)$$

where $R_1(\tau_e)$ is the synchronization coefficient of ED, i.e.,

$$R_1(\tau_e) = \int_{\tau_{\Omega_j^i, c_l^i}}^{\tau_{\Omega_j^i, c_l^i + 1}} p^2\left(t - \Omega_j^i T_f - c_l^i T_c + \tau_e\right) dt. \quad (20)$$

When the received signal is perfectly synchronized in the receiver, we have $R_0(0) = R_1(0) = 1$.

In the m-th chip of the k-th frame, where $m = 0, \ldots, M-1$, $k = 0, \ldots, L-1$, and $(m, k) \neq \left(\Omega_j^i, c_l^i\right)$, we have the detected CD and ED signals that are respectively given by

$$y_{c_{k,m}} = \sqrt{\rho E_p} n_{c_{k,m}}, \quad y_{e_{k,m}} = (1-\rho)\eta_{e_{k,m}}. \quad (21)$$

It is shown that $n_{c_{\Omega_j^i, c_l^i}}$, $n_{e_{\Omega_j^i, c_l^i}}$, $n_{c_{k,m}}$, and $n_{e_{k,m}}$ are Gaussian random variables following $\mathcal{N}\left(0, \frac{N_0}{2}\right)$. Note that the integral of $n_0^2(t)$ from ED in $t \in [\tau_{\Omega_j^i, c_l^i}, \tau_{\Omega_j^i, c_l^i + 1}]$ can be decomposed in a sum of approximately $2T_c W_{rx}$ independent random variables, where W_{rx} is the noise bandwidth that equals the bandwidth of the transmitted signal [22]. Since ultrasonic pulses are wideband signals, it is easy to achieve $2T_c W_{rx} > 40$. In this case, based on the central limit theorem, the distributions of $\eta_{e_{\Omega_j^i, c_l^i}}$ and $\eta_{e_{k,m}}$ are approximately

Gaussian [22], having a mean of cN_0 and a variance of cN_0^2, herein $c = T_c W_{rx}$.

Substituting (17), (19), and (21) into (11), we can write $y_{\Omega_j^i,c_l^i}$ and $y_{k,m}$ as

$$y_{\Omega_j^i,c_l^i} = hR_0(\tau_e)\sqrt{\rho}E_p + h^2R_1(\tau_e)(1-\rho)E_p + \sqrt{\rho E_p}n_{c_{\Omega_j^i,c_l^i}} + 2(1-\rho)h\sqrt{E_pR_1(\tau_e)}n_{e_{\Omega_j^i,c_l^i}} + (1-\rho)\eta_{e_{\Omega_j^i,c_l^i}}, \quad (22)$$

$$y_{k,m} = \sqrt{\rho E_p}n_{c_{k,m}} + (1-\rho)\eta_{e_{k,m}}. \quad (23)$$

Based on the aforementioned analysis, let

$$y_{\Omega_j^i,c_l^i} \sim \mathcal{N}\left(\mu_1, \sigma_1^2\right), \qquad y_{k,m} \sim \mathcal{N}\left(\mu_2, \sigma_2^2\right), \quad (24)$$

we can deduce that the mean and variance values are

$$\begin{aligned}
\mu_1 &= hR_0(\tau_e)\sqrt{\rho}E_p + h^2R_1(\tau_e)(1-\rho)E_p + (1-\rho)cN_0,\\
\mu_2 &= (1-\rho)cN_0,\\
\sigma_1^2 &= (1-\rho)^2cN_0^2 + \frac{\rho E_pN_0}{2} + 2(1-\rho)^2h^2E_pR_1(\tau_e)N_0 + \sigma_{\text{cov}}^2,\\
\sigma_2^2 &= \frac{\rho E_pN_0}{2} + (1-\rho)^2cN_0^2,
\end{aligned} \quad (25)$$

where σ_{cov}^2 represents the variance of correlated channel noise from CD and ED, i.e.,

$$\sigma_{\text{cov}}^2 = 4\sqrt{\rho}(1-\rho)hE_p\sqrt{R_1(\tau_e)}\mathbb{E}\left[n_{c_{\Omega_j^i,c_l^i}}n_{e_{\Omega_j^i,c_l^i}}\right]. \quad (26)$$

It is shown in (26) that the correlation of variables $n_{c_{\Omega_j^i,c_l^i}}$ and $n_{e_{\Omega_j^i,c_l^i}}$ will affect the distribution of the received signal in UsIM-S-MRC, leading to an impact on the system performance. To be specific, we analyze the TS and PS cases as follows.

1) TS CASE

The variables $n_{c_{\Omega_j^i,c_l^i}}$ and $n_{e_{\Omega_j^i,c_l^i}}$ are independent. We can calculate that

$$\sigma_{\text{cov}}^2 = 0. \quad (27)$$

2) PS CASE

Since CD and ED receive the signal simultaneously with different power levels, $n_{c_{\Omega_j^i,c_l^i}}$ and $n_{e_{\Omega_j^i,c_l^i}}$ represent the same channel noise, which means that the noises in CD and ED are completely correlated. Hence the variance σ_{cov}^2 in the PS case is calculated as

$$\begin{aligned}
\sigma_{\text{cov}}^2 &= 4\sqrt{\rho}(1-\rho)hE_p\sqrt{R_1(\tau_e)}\mathbb{E}\left[n_{c_{\Omega_j^i,c_l^i}}^2\right]\\
&= 2\sqrt{\rho}(1-\rho)hE_p\sqrt{R_1(\tau_e)}N_0.
\end{aligned} \quad (28)$$

Remark 2: According to (27) and (28), it can be found that compared with the TS case, an additional noise variance σ_{cov}^2 of the correlated channel noise is introduced in the PS case, leading to performance deterioration.

Then, according to (12), the detected CD and ED signals in each frame can be calculated as

$$y_{c_{\Omega_j^i}} = \sum_{m=0}^{M-1} y_{c_{\Omega_j^i,m}}, \qquad y_{e_{\Omega_j^i}} = \sum_{m=0}^{M-1} y_{e_{\Omega_j^i,m}}. \quad (29)$$

The integral of the Ω_j^i frame is rewritten as

$$y_{\Omega_j^i} = y_{c_{\Omega_j^i}} + y_{e_{\Omega_j^i}}. \quad (30)$$

Let the distribution of each frame be expressed as

$$y_{\Omega_j^i} \sim \mathcal{N}\left(\mu_{f1}, \sigma_{f1}^2\right), \qquad y_k \sim \mathcal{N}\left(\mu_{f2}, \sigma_{f2}^2\right), \quad (31)$$

where $k = 0, \ldots, L-1$, $k \neq \Omega_j^i$, the mean and variance values are given by

$$\begin{aligned}
&\mu_{f1} = \mu_1 + (M-1)\mu_2, \quad \sigma_{f1}^2 = \sigma_1^2 + (M-1)\sigma_2^2,\\
&\mu_{f2} = M\mu_2, \quad \sigma_{f2}^2 = M\sigma_2^2,
\end{aligned} \quad (32)$$

where μ_1, μ_2, σ_1^2, and σ_2^2 are given in (25), and σ_1^2 is related to (27) or (28).

Remark 3: From (32), we can observe that the correlated channel noise exists in only one of M ($M > 1$) chips in an active frame. Therefore, the joint design of UsIM and S-MRC can mitigate the impact of correlated channel noise by only detecting the active part of the transmission frames. To this end, S-MRC can always obtain performance gain over C-MRC in both TS and PS cases. In contrast, when using PS for the existing SDJD receiver [14], the correlated channel noise of CD and ED exists in the entire chip that is used for decision. The dominant effect of the correlated channel noise will degrade SDJD into the traditional CD receiver, resulting in no performance gain. Additionally, UsIM-S-MRC is superior to existing UsIM and SDJD systems in terms of BER, throughput, and complexity, which will be validated in Section IV.

B. BER

The average BER of UsIM-S-MRC is given by

$$P_b = \frac{p_1}{p_1+p_2}P_{em} + \frac{p_2}{p_1+p_2}P_{ei}, \quad (33)$$

where P_{em} is the average error probability of PPM bits, and P_{ei} is the average error probability of index bits. As long as we calculate P_{em} and P_{ei}, we can obtain P_b.

The P_{em} can be calculated as

$$P_{em} = P_{e1}(1-P_{ei}) + \frac{1}{2}P_{ei}, \quad (34)$$

where P_{e1} is the error probability of M-PPM. Further, the active frame combination can be erroneously detected as the remaining $2^{p_2}-1$ combinations. Since different detected active frame combinations correspond to the different numbers of erroneous index bits, we can calculate that $\mathbb{C}(p_2, p')$ error events correspond to p' erroneous index bits. Thus, P_{ei} is given by [23]

$$P_{ei} = \frac{P_{ed}}{p_2(2^{p_2}-1)}\sum_{p'=1}^{p_2} p'\mathbb{C}(p_2, p'), \quad (35)$$

where P_{ed} is the error probability of the active frame detection. According to (13), we have [24]

$$P_{ed} = 1 - \Pr\left(y_{\Omega_j} > \max_{\substack{k\in\{1,\ldots,2^{p_2}\}\\ k\neq j}} \left\{y_{\Omega_k}\right\}\right). \tag{36}$$

Resorting to the BER derivation of the MRC receiver in [11], P_{ed} can be rewritten as

$$P_{ed} = 1 - (1 - P_{e2})^{2^{p_2}-1}, \tag{37}$$

where

$$P_{e2} = \Pr\left(y_{\Omega_j^i} < y_k\right) = \mathbb{E}_h\left[Q\left(\frac{\mu_{f1} - \mu_{f2}}{\sqrt{\sigma_{f1}^2 + \sigma_{f2}^2}}\right)\right], \tag{38}$$

where y_k denotes the integral of an inactive frame; μ_{f1}, μ_{f2}, σ_{f1}^2, and σ_{f2}^2 are given in (32), and the specific values are determined by TS and PS. Referring to (25), (27), (28) and (32), we can sequentially calculate the P_{e2} of TS and PS as

$$P_{e2} = \begin{cases} \mathbb{E}_h\left[Q\left(\frac{(1-\rho)hR_1(\tau_e)+\sqrt{\rho}R_0(\tau_e)}{\sqrt{\frac{M\rho+2(1-\rho)^2h^2R_1(\tau_e)}{p\gamma}+\frac{2M(1-\rho)^2h^2c}{p^2\gamma^2}}}\right)\right], \\ \mathbb{E}_h\left[Q\left(\frac{(1-\rho)hR_1(\tau_e)+\sqrt{\rho}R_0(\tau_e)}{\sqrt{\frac{M\rho+2(1-\rho)^2h^2R_1(\tau_e)+2(1-\rho)h\sqrt{\rho}\sqrt{R_1(\tau_e)}}{p\gamma}+\frac{2M(1-\rho)^2h^2c}{p^2\gamma^2}}}\right)\right], \end{cases} \tag{39}$$

where $\gamma = h^2E_b/N_0$, denoting the signal-to-noise ratio (SNR) in the receiver, herein E_b is the energy of one bit and $E_b = KE_p/p$. After substituting (37) into (35), we obtain P_{ei}.

Next, suppose the first chip of the Ω_j^i frame is used, the probability of correctly detecting the pulse within the active frame is given by

$$P_{c1} = P\left(y_{\Omega_j^i,0} > y_{\Omega_j^i,1}, \ldots, y_{\Omega_j^i,0} > y_{\Omega_j^i,M-1} | \mathbf{x}_{\Omega_j^i,0} \text{ sent}\right). \tag{40}$$

Using different signal splitters, we can calculate P_{c1} as

$$P_{c1} = \int_{-\infty}^{\infty}\left(1 - Q\left(\frac{\sqrt{\rho}R_0(\tau_e) + (1-\rho)hR_1(\tau_e) + n - \frac{(1-\rho)hc}{p\gamma}}{\sqrt{\frac{\rho}{2p\gamma} + \frac{(1-\rho)^2h^2c}{p^2\gamma^2}}}\right)\right)^{M-1} p_{n_1}(n)dn, \tag{41}$$

where n_1 is given by

$$n_1 = \frac{\sqrt{\rho}n_{c_{\Omega_j^i,0}}}{h\sqrt{E_p}} + \frac{2(1-\rho)\sqrt{R_1(\tau_e)}n_{e_{\Omega_j^i,0}}}{\sqrt{E_p}} + \frac{(1-\rho)\eta_{e_{\Omega_j^i,0}}}{hE_p}, \tag{42}$$

and $p_{n_1}(n)$ is the PDF corresponding to TS or PS.

The error probability P_{e1} is calculated as [25]

$$P_{e1} = \frac{M}{2(M-1)}(1 - P_{c1}). \tag{43}$$

After substituting (35) and (43) into (34), we obtain P_{em}.

C. OPTIMAL SPLITTING RATIO

Since the closed-form P_{c1} for M-PPM is intractable [25], this subsection takes 2-PPM into account to derive the optimal splitting ratio. Suppose the received signal is perfectly synchronized in the receiver, according to the derivation of BER in Section III-B, we can deduce the optimal splitting ratio ρ^* of UsIM-S-MRC to achieve the lowest BER.

Proposition 1: Let us consider UsIM with 2-PPM. To achieve the lowest BER, the optimal splitting ratio in the TS case is in $\left[\rho_{TS2}^*, \rho_{TS1}^*\right]$, where

$$\rho_{TS2}^* = 1 + \frac{p\gamma\left(p\gamma - \sqrt{4h^2(2c+p\gamma)^2 + p^2\gamma^2}\right)}{2h^2(2c+p\gamma)^2}, \tag{44}$$

$$\rho_{TS1}^* = 1 + \frac{p\gamma\left(p\gamma - \sqrt{16h^2(c+p\gamma)^2 + p^2\gamma^2}\right)}{8h^2(c+p\gamma)^2}. \tag{45}$$

The optimal splitting ratio in the TS case for PPM-SDJD is ρ_{TS1}^*, as shown in (45).

Proof: See the Appendix. ■

Proposition 2: In the PS case, let us consider UsIM with 2-PPM again. To achieve the lowest BER, the optimal splitting ratio for S-MRC is in $(\rho_{PS2}^*, 1)$, where

$$\rho_{PS2}^* = 1 + \frac{p\gamma\left(p\gamma - \sqrt{4h^2(4c+p\gamma)^2 + p^2\gamma^2}\right)}{2h^2(4c+p\gamma)^2}. \tag{46}$$

The optimal splitting ratio for PPM-SDJD is $\rho_{PS1}^* = 1$.

In the TS case, since the values of ρ_{TS1}^* and ρ_{TS2}^* are within $(0, 1)$, the optimal splitting ratios of S-MRC and SDJD are in $(0, 1)$. Therefore, S-MRC and SDJD can improve BER performance compared with the CD (i.e., $\rho = 1$) and ED (i.e., $\rho = 0$) receivers. In the PS case, it can be derived that the SDJD receiver degrades into a CD receiver since the ρ^* equals 1. In contrast, benefiting from the joint design of UsIM and S-MRC, the optimal splitting ratio of S-MRC is $\rho_{PS2}^* \in (0, 1)$, and thus attains performance gain over C-MRC (i.e., $\rho = 1$), showing the superiority of UsIM-S-MRC over PPM-SDJD.

D. MUTUAL INFORMATION

Let a set $\mathbf{X} = \{\mathbf{x}_{\Omega_j,c_l}\}$ represent all possible transmission vectors. Each element in $\mathbf{X}$ is transmitted with equal probabilities, where $j = 1, \ldots, 2^{p_2}$ and $l = 1, \ldots, M^K$. From the perspective of information theory, the mutual information of UsIM-S-MRC in terms of bits per channel use (bpcu) is calculated as [26]

$$\begin{aligned} \mathrm{I}(\mathbf{x}; \mathbf{y}) &= \mathrm{H}(\mathbf{x}) - \mathbb{E}_h[\mathbf{x}|\mathbf{y}, h] \\ &= \log_2\left(2^{p_2}M^K\right) - \mathbb{E}_h[\mathbf{x}|\mathbf{y}, h], \end{aligned} \tag{47}$$

where $\mathbf{x} \in \mathbf{X}$ and $\mathbb{E}_h[\mathbf{x}|\mathbf{y}, h]$ is given by [27]

$$\mathbb{E}_h[\mathbf{x}|\mathbf{y}, h] = -\sum_{j=1}^{2^{p_2}} \sum_{l=1}^{M^K} \int_{\mathbf{y}} \Pr\left(\mathbf{x}_{\Omega_j,c_l}\right) f\left(\mathbf{y}|\mathbf{x}_{\Omega_j,c_l}\right) \times \log_2\left(\frac{\Pr\left(\mathbf{x}_{\Omega_j,c_l}\right) f\left(\mathbf{y}|\mathbf{x}_{\Omega_j,c_l}\right)}{f(\mathbf{y}|h)}\right) d\mathbf{y}. \quad (48)$$

The conditional PDF $f\left(\mathbf{y}|\mathbf{x}_{\Omega_j,c_l}\right)$ is given by [28]

$$f\left(\mathbf{y}|\mathbf{x}_{\Omega_j,c_l}\right) = \left(2\pi\sigma_1^2\right)^{\frac{K}{2}} \left(2\pi\sigma_2^2\right)^{\frac{LM-K}{2}} \times \prod_{i=1}^{K} \exp\left(-\frac{\left(y_{\Omega_j^i,c_l^i} - \mu_1\right)^2}{2\sigma_1^2}\right) \times \prod_{k=0}^{L-1} \prod_{m=0}^{M-1} \exp\left(-\frac{\left(y_{k,m} - \mu_2\right)^2}{2\sigma_2^2}\right), \quad (49)$$

where $(k, m) \neq \left(\Omega_j^i, c_l^i\right)$, and the mean and variance values are given in (25). The conditional PDF $f(\mathbf{y}|h)$ can be calculated as

$$\begin{aligned} f(\mathbf{y}|h) &= \sum_{j'=1}^{2^{p_2}} \sum_{l'=1}^{M^K} \Pr\left(\mathbf{x}_{\Omega_{j'},c_{l'}}\right) f\left(\mathbf{y}|\mathbf{x}_{\Omega_{j'},c_{l'}}\right) \\ &= \frac{1}{2^{p_2} M^K} \sum_{j'=1}^{2^{p_2}} \sum_{l'=1}^{M^K} \left(2\pi\sigma_1^2\right)^{\frac{K}{2}} \left(2\pi\sigma_2^2\right)^{\frac{LM-K}{2}} \\ &\quad \times \prod_{i=1}^{K} \exp\left(-\frac{\left(y_{\Omega_{j'}^i,c_{l'}^i} - \mu_1\right)^2}{2\sigma_1^2}\right) \\ &\quad \times \prod_{k'=0}^{L-1} \prod_{m'=0}^{M-1} \exp\left(-\frac{\left(y_{k',m'} - \mu_2\right)^2}{2\sigma_2^2}\right), \end{aligned} \quad (50)$$

where $(k', m') \neq \left(\Omega_{j'}^i, c_{l'}^i\right)$. According to (49) and (50), we obtain

$$\begin{aligned} &-\log_2\left(\frac{\Pr\left(\mathbf{x}_{\Omega_j,c_l}\right) f\left(\mathbf{y}|\mathbf{x}_{\Omega_j,c_l}\right)}{f(\mathbf{y}|h)}\right) \\ &= \log_2\left(\sum_{j'=1}^{2^{p_2}} \sum_{l'=1}^{M^K} \exp\left(\frac{\sum_{i=1}^{K}\left(y_{\Omega_j^i,c_l^i} - \mu_1\right)^2 - \left(y_{\Omega_{j'}^i,c_{l'}^i} - \mu_1\right)^2}{2\sigma_1^2}\right.\right. \\ &\quad \left.\left. + \frac{\sum_{k=0}^{L-1}\sum_{m=0}^{M-1}\left(y_{k,m} - \mu_2\right)^2 - \sum_{k'=0}^{L-1}\sum_{m'=0}^{M-1}\left(y_{k',m'} - \mu_2\right)^2}{2\sigma_2^2}\right)\right), \end{aligned} \quad (51)$$

where $(k, m) \neq \left(\Omega_j^i, c_l^i\right)$ and $(k', m') \neq \left(\Omega_{j'}^i, c_{l'}^i\right)$. By substituting (49) and (51) into (48), we obtain the mutual information of UsIM-S-MRC as

$$\mathrm{I}(\mathbf{x}; \mathbf{y}) = \log_2\left(2^{p_2} M^K\right) - \mathbb{E}_{\mathbf{y}|\mathbf{x}_{\Omega_1,c_1}}\left[\log_2\left(\xi\left(\mathbf{y}|\mathbf{x}_{\Omega_1,c_1}\right)\right)\right], \quad (52)$$

where $\mathbb{E}_{\mathbf{y}|\mathbf{x}_{\Omega_1,c_1}}[\cdot]$ is the expectation with respect to $\mathbf{y}|\mathbf{x}_{\Omega_1,c_1}$, and $\xi\left(\mathbf{y}|\mathbf{x}_{\Omega_1,c_1}\right)$ is given by

$$\begin{aligned} &\xi\left(\mathbf{y}|\mathbf{x}_{\Omega_1,c_1}\right) \\ &= \sum_{j'=1}^{2^{p_2}} \sum_{l'=1}^{M^K} \exp\left(\frac{\sum_{i=1}^{K}\left(y_{\Omega_1^i,c_1^i} - \mu_1\right)^2 - \left(y_{\Omega_{j'}^i,c_{l'}^i} - \mu_1\right)^2}{2\sigma_1^2}\right. \\ &\quad \left. + \frac{\sum_{k=0}^{L-1}\sum_{m=0}^{M-1}\left(y_{k,m} - \mu_2\right)^2 - \sum_{k'=0}^{L-1}\sum_{m'=0}^{M-1}\left(y_{k',m'} - \mu_2\right)^2}{2\sigma_2^2}\right), \end{aligned} \quad (53)$$

where μ_1, μ_2, σ_1^2, and σ_2^2 are given in (25), and it can be inferred from (25) that the mutual information is associated with the power splitting ratio ρ. Furthermore, since the values of σ_1^2 and σ_2^2 are determined by the specific signal splitters as analyzed in Section III-A, the mutual information is affected by the TS and PS splitters.

Note that in the case of $K = 1$, Eq. (52) calculates the mutual information of 2^p-PPM, and herein $\xi\left(\mathbf{y}|\mathbf{x}_{\Omega_1,c_1}\right)$ is simplified as

$$\xi\left(\mathbf{y}|\mathbf{x}_{\Omega_1,c_1}\right) = \sum_{j'=1}^{2^p} \exp\left[\frac{\left(y_{\Omega_1^1,c_1^1} - \mu_1\right)^2 - \left(y_{\Omega_{j'}^1,c_1^1} - \mu_1\right)^2}{2\sigma_1^2} + \frac{\left(y_{\Omega_{j'}^1,c_1^1} - \mu_2\right)^2 - \left(y_{\Omega_1^1,c_1^1} - \mu_2\right)^2}{2\sigma_2^2}\right]. \quad (54)$$

Remark 4: In the case that K is a constant, increasing M and L will increase p_1 and p_2 respectively. Thus, the source entropy of UsIM, i.e., $\mathrm{H}(\mathbf{x})$, will be enhanced and it is beneficial to obtain higher mutual information according to (47). Particularly, in the case of $K = 1$, the source entropy of both UsIM and 2^p-PPM is p. UsIM may achieve higher mutual information within the same duration as 2^p-PPM by activating K' ($K' > 1$) frames to reach a source entropy of $p + (K' - 1)\log_2 M$. This is because UsIM not only uses the frame index to convey information bits, but also transmits PPM bits within the active frames. While 2^p-PPM only transmits information bits within frames. Therefore, the joint-designed UsIM-S-MRC system is beneficial to achieve higher mutual information than 2^p-PPM, which can provide higher achievable rates for versatile IBC applications.

Remark 5: In the case of $K < L$, the source entropy of UsIM is $p_2 + K\log_2 M$. In the case of $K = L$, all frames use M-PPM to transmit PPM bits and the source entropy becomes $L\log_2 M$. When UsIM and M-PPM adopt the same frame duration, since UsIM activates a part of transmission frames, M-PPM can achieve higher mutual information than UsIM. However, the successive ultrasonic pulse transmission may cause severe heat dissipation [3] that is harmful to vulnerable organs and tissues in the human body. Thus, to

maintain low duty cycle ultrasonic pulses for the safety of the human body, it is not necessary to activate more than half of the frames. Moreover, M-PPM has to transmit pulses with a large chip width to maintain a low duty cycle and thus sacrifice the data rate. Therefore, UsIM can attain low duty cycle pulses and achieve high data rates by transmitting additional index bits without transmitting additional pulses.

E. THROUGHPUT

The throughput is defined as the average number of correctly received bits in unit time [11]. Thus, the throughput of UsIM is calculated as

$$R_{t_{\mathrm{UsIM}}} = \frac{(1 - BER_{\mathrm{UsIM}})p}{LMT_c}. \tag{55}$$

As long as S-MRC achieves lower BER than C-MRC, S-MRC can obtain higher throughput than C-MRC. Furthermore, the throughput of PPM-SDJD is given by

$$\begin{aligned} R_{t_{\mathrm{SDJD}}} &= \frac{(1 - BER_{\mathrm{SDJD}})\log_2 M}{MT_c} \\ &= \frac{(1 - BER_{\mathrm{SDJD}})\big(p + (L-K)\log_2 M - p_2\big)}{LMT_c}. \end{aligned} \tag{56}$$

Comparing (55) and (56), when the BER of UsIM-S-MRC is lower than that of PPM-SDJD, and the number of index bits p_2 is higher than $(L-K)\log_2 M$, the proposed UsIM-S-MRC can achieve higher throughput than PPM-SDJD.

IV. SIMULATION RESULTS

In this section, extensive Monte Carlo simulations are performed to study the performance of UsIM-S-MRC in terms of mutual information, BER, optimal splitting ratio, and throughput in both TS and PS cases. The channel state information is assumed to be perfectly known at all considered receivers. The maximum transmission power is set to 16 μW (i.e., SNR = 12 dB) over a transducer area of 1 cm^2, which is below the maximum limit (720 mW/cm^2) imposed by the FDA [6], [7]. The timing synchronization error τ_e is assumed to follow a Tikhonov distribution [29], which is expressed as

$$f(\tau_e) = \frac{1}{2\pi I_0\left(\frac{1}{\sigma_{\tau_e}^2}\right)} \exp\left(\frac{\cos\tau_e}{\sigma_{\tau_e}^2}\right), \tag{57}$$

where σ_{τ_e} denotes the standard deviation of τ_e.

At the receiver end, we compare the S-MRC receiver with the C-ML and C-MRC receivers for UsIM to demonstrate the superiority of S-MRC. At the transmitter end, we compare UsIM using S-MRC with PPM using SDJD to show the superiority of the joint design of UsIM-S-MRC for IBCs. In all simulations, unless stated otherwise, the received signal is perfectly synchronized with the template signal in CD. The transmitters use 2-PPM (i.e., $M = 2$). The channel attenuation is assumed to be normalized in all receivers and the channel fading follows the generalized Nakagami fading in (5), where the shaping, spreading, and generalization parameters are $\alpha = 0.59$, $\beta = 0.05$, and $z = 1.12$, respectively [7], [20].

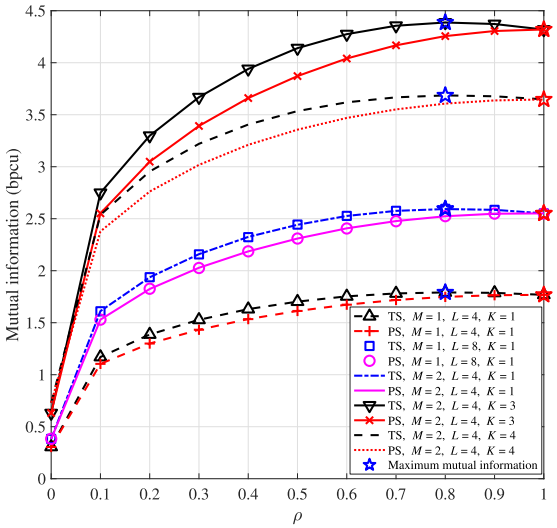

FIGURE 4. Mutual information of UsIM-S-MRC versus the splitting ratio ρ in the cases of $M = 1, 2$, $L = 4, 8$, and $K = 1, 3, 4$ at the SNR = 6 dB in the TS and PS cases.

A. MUTUAL INFORMATION FOR S-MRC

Figure 4 shows mutual information of UsIM-S-MRC versus the splitting ratio ρ in the cases of $M = 1, 2$, $L = 4, 8$, and $K = 1, 3, 4$ at the SNR = 6 dB in the TS and PS cases. It can be observed that S-MRC can always achieve better mutual information in the TS case than in the PS case, indicating that TS can help S-MRC to achieve higher data rates. This is due to the independent noises in CD and ED in the TS case. In the PS case, the maximum mutual information is achieved at the value of $\rho = 1$ and thus S-MRC cannot obtain mutual information gain. This is due to the correlated channel noise of CD and ED, validating *Remark 2*. It is worth noting that when $\rho = 1$, S-MRC degrades into C-MRC in the PS case. Moreover, when $K = 1$, in the cases of $M = 1$, $L = 8$ (i.e., $p_1 = 0$, $p_2 = 3$) and $M = 2$, $L = 4$ (i.e., $p_1 = 1$, $p_2 = 2$), the same mutual information is achieved in the TS or PS case. This is because when $K = 1$, the mutual information of the two curves is equivalent to that of 8-PPM.

Let us compare the curves of $\{M = 2,\ L = 4,\ K = 3\}$ and $\{M = 2,\ L = 4,\ K = 4\}$ in Fig. 4. We can observe that the mutual information in $K = 3$ is higher than that in $K = 4$. This is because when $K = 3$, three PPM bits and two index bits are transmitted, while when $K = 4$, all frames in one block are used to transmit four PPM bits. Therefore, higher source entropy and mutual information can be obtained when $K = 3$, benefiting from the UsIM transmission. Furthermore, the maximum mutual information in the TS case is achieved at $\rho \in (0, 1)$. This means that using TS at S-MRC can further attain performance gain in terms of mutual information compared with C-MRC.

Since no performance gain in terms of mutual information exists in the PS case, we next compare the mutual information of UsIM-S-MRC with existing UsIM and PPM-SDJD in the TS case. Fig. 5 depicts the mutual information of UsIM-S-MRC, UsIM using C-MRC, and PPM-SDJD

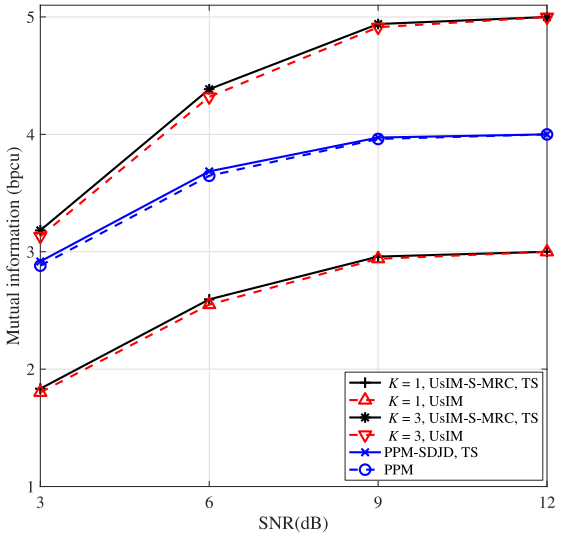

FIGURE 5. Mutual information of UsIM-S-MRC, UsIM using C-MRC, and PPM-SDJD versus SNR in the cases of $M = 2$, $L = 4$, and $K = 1, 3$ in the TS case.

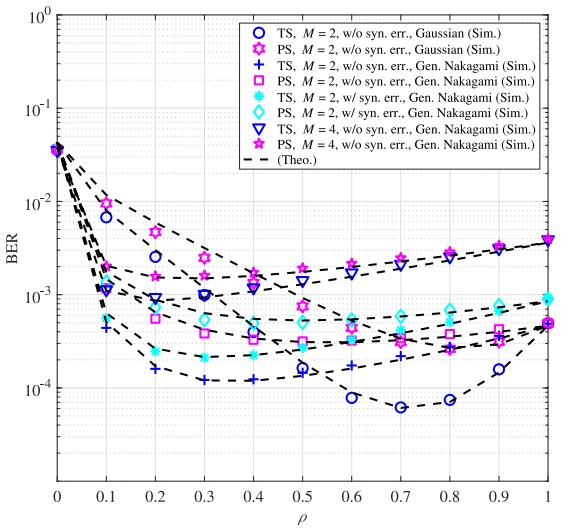

FIGURE 6. Theoretical and simulation BER of S-MRC versus the splitting ratio ρ in the cases of $K = 1$, $p_1 = 1, 2$ (i.e., $M = 2, 4$), $p_2 = 2$ (i.e., $L = 4$), and SNR = 9 dB, in the TS and PS cases, over the Gaussian (i.e., $|h| = 1$) and generalized Nakagami channels in the UsIM-S-MRC systems without and with synchronization errors of $\sigma_{\tau_e} = 0, 0.01$.

versus SNR in the cases of $M = 2$, $L = 4$, and $K = 1, 3$. It can be observed that the splitting receivers (i.e., S-MRC and SDJD) employing TS can attain performance gain regardless of whether the transmitter adopts PPM or UsIM. Note that the two curves in the same case converge at high SNR. This can be explained from the information-theoretical perspective, i.e., the uncertainty of the received signal decreases as the SNR increases and thus the mutual information almost reaches the source entropy.

B. BER ANALYSIS FOR USIM-S-MRC

Figure 6 depicts the theoretical and simulation BER of S-MRC versus the splitting ratio ρ in the cases of $K = 1$, $p_1 = 1, 2$ (i.e., $M = 2, 4$), $p_2 = 2$ (i.e., $L = 4$), and

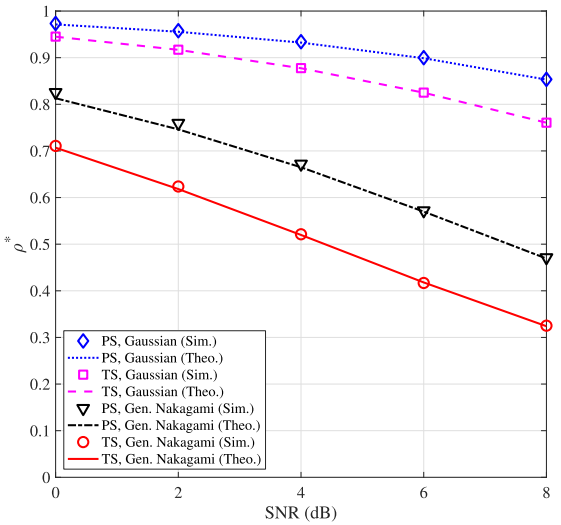

FIGURE 7. Theoretical and simulation optimal splitting ratio ρ^* of UsIM-S-MRC versus SNR in the cases of $p_1 = 1$ (i.e., $K = 1$) and $p_2 = 2$ (i.e., $L = 4$) with TS and PS, over the Gaussian and generalized Nakagami channels.

SNR = 9 dB, in the TS and PS cases, over the Gaussian (i.e., $|h| = 1$) and generalized Nakagami channels in the UsIM-S-MRC systems without and with synchronization errors of $\sigma_{\tau_e} = 0, 0.01$. It can be observed that when ρ is close to zero, the theoretical curves are slightly higher than the simulation ones. This is due to the Gaussian approximation of the square-noise of ED. As ρ increases to one, the theoretical curves agree with the simulation counterparts well, which validates the theoretical BER derivation in Section III-B. Moreover, we can find that for both TS and PS cases, the lowest BER of S-MRC is achieved at a value of $\rho \in (0, 1)$, which jointly uses CD and ED, neither at $\rho = 0$ nor $\rho = 1$ (i.e., C-MRC). This observation can also be theoretically explained by *Propositions 1 and 2*. Additionally, although the timing synchronization errors degrade BER performance, the performance gains still exist.

In Fig. 6, comparing the BER curves in the TS case with the counterparts in the PS case, it is obvious that S-MRC using TS can always achieve lower BERs than using PS. This observation is consistent with the results in Fig. 4. The higher BER in the PS case is inevitable due to the correlated channel noise of CD and ED. The higher modulation order M leads to higher BER due to the increased accumulated noise in the frames. Besides, to achieve the lowest BER, more power is allocated to ED in fading channels compared with the counterparts in Gaussian channels. This is because CD is severely impaired by channel fading while ED is more robust in fading channels. Although channel fading affects the value of the optimal splitting ratio for the lowest BER, the BER gain still exists, showing the superiority of S-MRC in both Gaussian and intra-body fading channels.

Figure 7 depicts the theoretical and simulation optimal splitting ratio ρ^* of UsIM-S-MRC versus SNR in the cases of $p_1 = 1$ (i.e., $K = 1$) and $p_2 = 2$ (i.e., $L = 4$) with TS and PS, over the Gaussian and generalized Nakagami

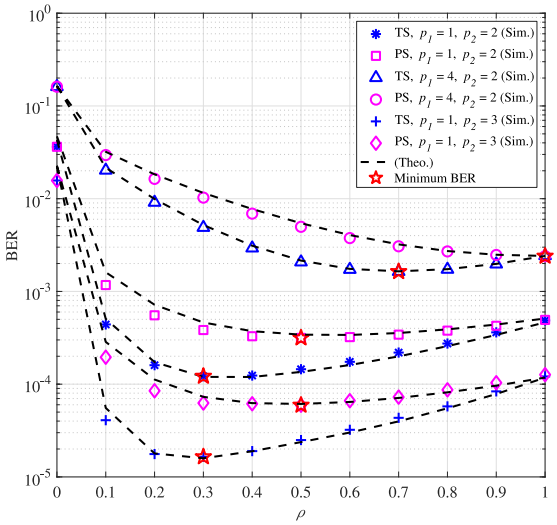

FIGURE 8. Theoretical and simulation BER of UsIM-S-MRC versus the splitting ratio ρ in the cases of $p_1 = 1, 4$ (i.e., $K = 1, 4$), $p_2 = 2, 3$ (i.e., $L = 4, 8$), and SNR = 9 dB in the TS and PS cases.

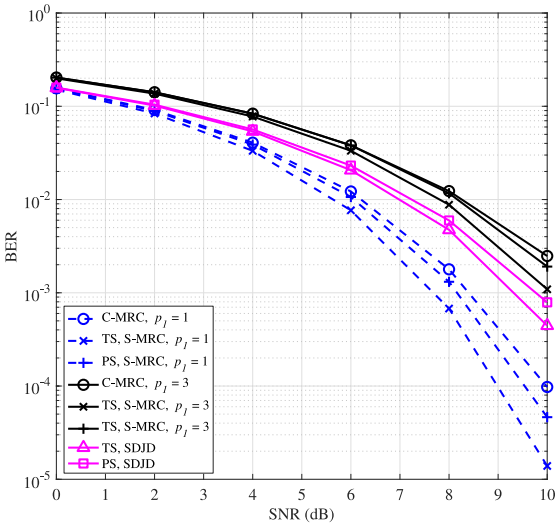

FIGURE 9. BER of S-MRC and SDJD versus SNR in the cases of $p_1 = 1, 3$ (i.e., $K = 1, 3$) and $p_2 = 2$ (i.e., $L = 4$) in the TS and PS cases.

channels. The theoretical ρ^* is calculated by (44) and (46). The simulation ρ^* is measured at the lowest BERs. We can observe that the theoretical results agree with the simulation counterparts well, and thus *Propositions 1 and 2* are verified. We can also observe that ρ^* in the PS case is higher than that in the TS case. This is because PS induces the correlated channel noise, and more power is allocated to CD to alleviate the impact of correlated channel noise. Moreover, we can find that ρ^* over Gaussian channels is higher than the counterpart over generalized Nakagami channels. The reason is that channel fading has a more serious effect on CD than ED, more power is allocated to ED over generalized Nakagami channels compared with Gaussian channels.

Next, let us analyze how p_1 and p_2 affect the BER performance of S-MRC in the TS and PS cases. Fig. 8 depicts the theoretical and simulation BER of UsIM-S-MRC versus the splitting ratio ρ in the cases of $p_1 = 1, 4$ (i.e., $K = 1, 4$), $p_2 = 2, 3$ (i.e., $L = 4, 8$), and SNR $= 9$ dB in the TS and PS cases. It can be observed that the BER in the TS case at the optimal splitting ratio can reach around 10^{-5}, which is more than one order of magnitude lower than the corresponding BER using a CD (i.e., $\rho = 1$). In the case of $p_2 = 2$, BER becomes higher as p_1 increases. In the case of $p_1 = 1$, BER becomes lower as p_2 increases. The reason is that to maintain the same SNR, the increased p_1 significantly increases accumulated noise and slightly increases the pulse energy, while the increased p_2 can enhance the pulse energy without inducing additional noise. Moreover, the BER gains of the minimum BER of TS to that of PS are respectively about 4.14 dB, 1.66 dB, and 5.56 dB in the cases of $\{p_1 = 1,\ p_2 = 2\}$, $\{p_1 = 4,\ p_2 = 2\}$, and $\{p_1 = 1,\ p_2 = 3\}$. Taking the BER gain of 4.14 dB as a benchmark, it can be concluded that the BER gain of TS to PS becomes higher with the increase of p_2 or the decrease of p_1. Therefore, the impact of the correlated channel noise of PS becomes weaker as p_1 increases or as p_2 decreases.

Notice that in Fig. 8, when $p_1 = 4$ (i.e., $K = 4$), all chips are used to transmit PPM bits, and UsIM-S-MRC degrades into PPM-SDJD. It is obvious that in the PS case, SDJD has no BER gain, which shows different results from the existing research [14]. These observations agree with *Remark 3*. Since UsIM and S-MRC can disperse the correlated channel noise of CD and ED in one chip to the whole active frame, BER gain can be obtained in both TS and PS cases. While for PPM-SDJD, the correlated channel noise exists in the entire decision chip. Moreover, S-MRC in the PS case achieves lower BER than that of SDJD in both TS and PS cases. Therefore, the joint design of UsIM-S-MRC can implement an ultrasonic IBC system with a much lower BER and complexity than the existing SDJD.

C. COMPARISON OF USIM-S-MRC WITH USIM AND SDJD

In this section, we perform extensive simulations to further reveal the superiority of UsIM-S-MRC over existing UsIM [11] and PPM-SDJD [14]. For fairness, PPM-SDJD uses the same chip duration as UsIM-S-MRC and UsIM. Thus, PPM-SDJD can transmit four modulated bits by four pulses in one block duration.

Figure 9 depicts the simulation BER of S-MRC and SDJD versus SNR in the cases of $p_1 = 1, 3$ (i.e., $K = 1, 3$) and $p_2 = 2$ (i.e., $L = 4$) in the TS and PS cases. The BERs of the S-MRC receiver are measured at the optimal splitting ratios, which achieve the lowest BERs. It can be observed that the BER of SDJD is higher than that of S-MRC in the case of $p_1 = 1$ (i.e., $K = 1$) and lower than that of S-MRC in the case of $p_1 = 3$ (i.e., $K = 3$). This can be explained by two facts. On the one hand, adopting UsIM with $p_1 = 1$, one ultrasonic pulse can convey three bits, while 2-PPM transmits one bit by one ultrasonic pulse. Consequently,

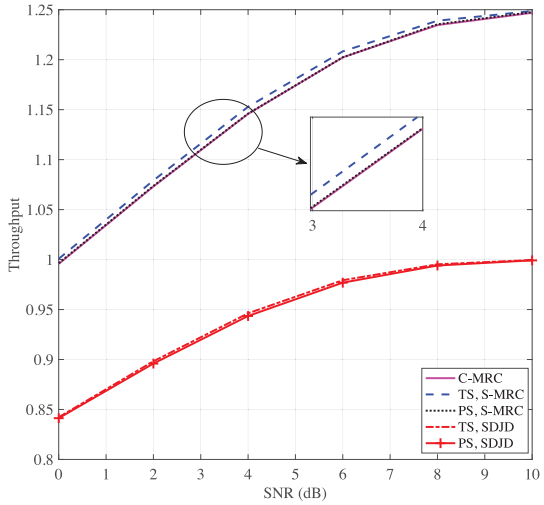

FIGURE 10. Throughput of C-MRC, S-MRC, and SDJD versus SNR in the cases of $p_1 = 3$ (i.e., $K = 3$) and $p_2 = 2$ (i.e., $L = 4$) in the TS and PS cases.

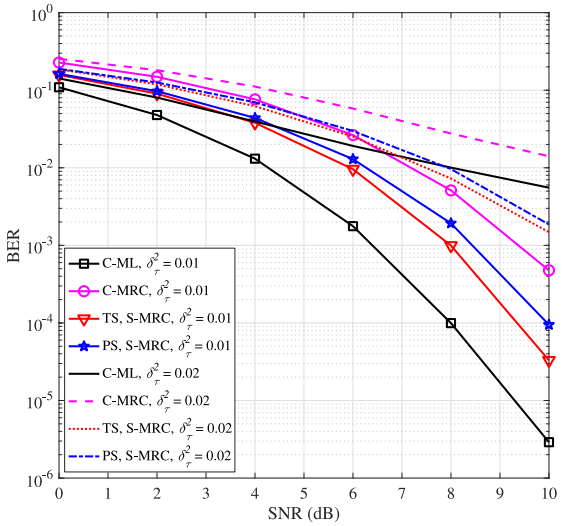

FIGURE 11. BER of C-ML, C-MRC, S-MRC with TS and S-MRC with PS versus SNR in the cases of $p_1 = 1$ (i.e., $K = 1$) and $p_2 = 2$ (i.e., $L = 4$), in the UsIM-S-MRC systems with synchronization errors of $\delta_{\tau_e} = 0.01, 0.02$.

with the same SNR, one pulse in UsIM has much higher pulse energy than that in 2-PPM. The corresponding S-MRC can achieve much lower BER than SDJD. On the other hand, to maintain the same SNR, the increased p_1 lowers the average pulse energy in UsIM and thus increases BER.

Figure 10 depicts the throughput of C-MRC, S-MRC, and SDJD versus SNR in the cases of $p_1 = 3$ (i.e., $K = 3$) and $p_2 = 2$ (i.e., $L = 4$) in the TS and PS cases. The throughput for all schemes is normalized as the correctly received bits per frame. Obviously, S-MRC has a higher throughput than that of SDJD, benefiting from the high data rate of UsIM. Since UsIM transmits five bits within one block duration, while SDJD only transmits four bits per block. Furthermore, for both S-MRC and SDJD, the throughput in the TS case is slightly higher than that in the PS case. The throughput improvement of TS to PS in S-MRC is greater than that in SDJD, showing the superiority of UsIM-S-MRC in reducing average channel noise. Besides, although UsIM provides high throughput, S-MRC with TS can still improve the throughput of the existing C-MRC slightly. Therefore, UsIM-S-MRC can achieve higher throughput than existing UsIM and SDJD systems with low complexity.

Next, to show the superiority of the joint design of UsIM and S-MRC, Fig. 11 compares the simulation BER of C-ML, C-MRC, S-MRC with TS and S-MRC with PS versus SNR in the cases of $p_1 = 1$ (i.e., $K = 1$) and $p_2 = 2$ (i.e., $L = 4$), in the UsIM-S-MRC systems with synchronization errors of $\delta_{\tau_e} = 0.01, 0.02$. We can see that the S-MRC receiver in both TS and PS cases achieves lower BERs compared with C-MRC, benefiting from the diversity combing from CD and ED [14]. When $\delta_{\tau_e} = 0.02$, the BERs of C-ML and C-MRC deteriorate seriously since the performance of CD highly depends on synchronization accuracy. Although S-MRC also deteriorates in the case of $\delta_{\tau_e} = 0.02$, it achieves lower BER than C-ML and C-MRC. This is expected since S-MRC benefits from the signal splitter jointly using CD and ED.

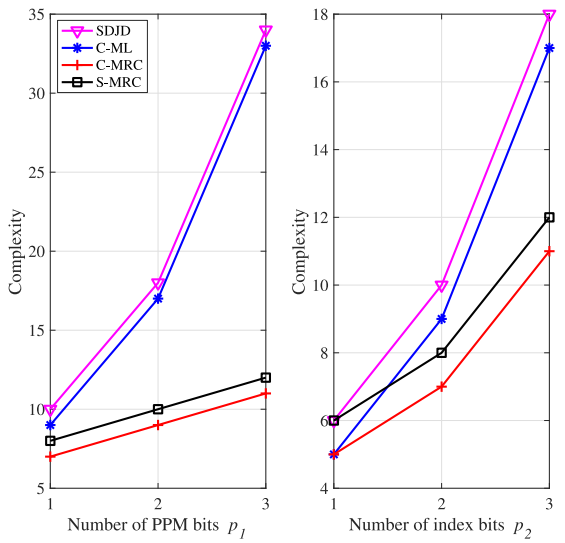

FIGURE 12. Complexity comparison among C-ML, C-MRC, S-MRC, and SDJD (left) versus the number of PPM bits p_1 in the case of $p_2 = 2$ (i.e., $L = 4$), and (right) versus the number of index bits p_2 in the case of $p_1 = 1$ (i.e., $K = 1$).

Finally, to compare the complexity of all receivers, Fig. 12 shows the complexity comparison among the C-ML, C-MRC, and S-MRC for UsIM and SDJD for 2^p-PPM. We can find that to transmit the same number of information bits, C-MRC has the lowest complexity, and S-MRC has lower complexity than C-ML and SDJD. Although the complexity of S-MRC is slightly higher than that of C-MRC due to the joint use of CD and ED, S-MRC can significantly improve the BER performance compared with C-MRC, as shown in Figs. 9 and 11. Therefore, S-MRC can achieve lower complexity than C-ML and lower BER than C-MRC, which

provides a suitable trade-off between BER and complexity for the existing UsIM.

V. CONCLUSION

This paper revealed the critical impact of channel noise correlation on ultrasonic splitting receivers. To attain performance gains in terms of mutual information and BER for ultrasonic IBCs, we proposed a UsIM-S-MRC system to mitigate the impact of channel noise correlation. We further derived the theoretical mutual information, BER, and optimal splitting ratio of UsIM-S-MRC considering timing synchronization error. Extensive Monte Carlo simulations verified the theoretical analysis and showed that S-MRC with TS can achieve higher mutual information and lower BER than S-MRC with PS due to the independent channel noises in CD and ED. More importantly, the joint-designed UsIM-S-MRC system can achieve lower BER and higher throughput than existing PPM-SDJD, and can achieve lower BER than C-ML and C-MRC receivers in UsIM systems with synchronization errors, providing a robust and superior solution for IBCs. Our future work will focus on designing coding schemes and splitting schemes for UsIM-S-MRC to further improve the performance.

APPENDIX
PROOF OF PROPOSITION 1

Referring to (33), to obtain the lowest P_b, it is necessary to lower the error probabilities of PPM bits and index bits, which are associated with P_{e1} and P_{e2} according to (34)–(38). To this end, the optimal splitting ratio ρ^* should minimize P_{e1} and P_{e2} simultaneously. Since the closed-from error probability P_{e1} for M-PPM is intractable, we analyze 2-PPM in perfectly synchronized UsIM systems.

In the TS case, we can derive P_{e1} conditioned on the channel coefficient h as

$$\begin{aligned} P_{e1} &= \frac{1}{2}P\left(y_{\Omega_j^i,1} > y_{\Omega_j^i,0}|\mathbf{x}_{\Omega_j^i,0}\text{ sent}\right) \\ &\quad + \frac{1}{2}P\left(y_{\Omega_j^i,0} > y_{\Omega_j^i,1}|\mathbf{x}_{\Omega_j^i,1}\text{ sent}\right) \\ &= Q\left(\frac{(1-\rho)h+\sqrt{\rho}}{\sqrt{\frac{\rho+2(1-\rho)^2h^2}{p\gamma}+\frac{2(1-\rho)^2h^2c}{p^2\gamma^2}}}\right). \end{aligned} \tag{58}$$

Let $P_{e1} = Q(R_{TS1})$, we have

$$R_{TS1} = \frac{(1-\rho)h+\sqrt{\rho}}{\sqrt{\frac{\rho+2(1-\rho)^2h^2}{p\gamma}+\frac{2(1-\rho)^2h^2c}{p^2\gamma^2}}}. \tag{59}$$

By substituting $M = 2$ into (39), we have P_{e2} conditioned on the channel coefficient h as $P_{e2} = Q(R_{TS2})$, where

$$R_{TS2} = \frac{(1-\rho)h+\sqrt{\rho}}{\sqrt{\frac{2\rho+2(1-\rho)^2h^2}{p\gamma}+\frac{4(1-\rho)^2h^2c}{p^2\gamma^2}}}. \tag{60}$$

Since the Gaussian Q-function is monotonically decreasing, minimizing $Q(R)$ is equivalent to maximizing R. Therefore, to decrease P_{e1} and P_{e2}, we need to increase R_{TS1} and R_{TS2}.

The derivative of R_{TS1} with respect to ρ is calculated as

$$\frac{\partial R_{TS1}}{\partial \rho} = \frac{h(1+\rho)\left(2ch(1-\rho)+p\gamma\left(2h(1-\rho)-\sqrt{\rho}\right)\right)}{2p^2\gamma^2\sqrt{\rho}\left(\frac{2ch^2(1-\rho)^2+p\gamma\left(2h^2(1-\rho)^2+\rho\right)}{p^2\gamma^2}\right)^{\frac{3}{2}}}. \tag{61}$$

The derivative of R_{TS2} with respect to ρ is calculated as

$$\frac{\partial R_{TS2}}{\partial \rho} = \frac{h(1+\rho)\left(2ch(1-\rho)+p\gamma\left(h(1-\rho)-\sqrt{\rho}\right)\right)}{2\sqrt{2}p^2\gamma^2\sqrt{\rho}\left(\frac{2ch^2(1-\rho)^2+p\gamma\left(h^2(1-\rho)^2+\rho\right)}{p^2\gamma^2}\right)^{\frac{3}{2}}}. \tag{62}$$

Let $\frac{\partial R_{TS1}}{\partial \rho} = 0$ and $\frac{\partial R_{TS2}}{\partial \rho} = 0$, we obtain ρ^*_{TS1} and ρ^*_{TS2} that are given in (45) and (44). Since

$$\begin{cases} \frac{\partial R_{TS1}}{\partial \rho} > 0, & \frac{\partial R_{TS2}}{\partial \rho} > 0, \ \rho \in \left[0, \rho^*_{TS2}\right), \\ \frac{\partial R_{TS1}}{\partial \rho} > 0, & \frac{\partial R_{TS2}}{\partial \rho} < 0, \ \rho \in \left(\rho^*_{TS2}, \rho^*_{TS1}\right), \\ \frac{\partial R_{TS1}}{\partial \rho} < 0, & \frac{\partial R_{TS2}}{\partial \rho} < 0, \ \rho \in \left(\rho^*_{TS1}, 1\right], \end{cases} \tag{63}$$

to obtain the maximum R_{TS1} and the maximum R_{TS2}, the optimal splitting ratio is given by

$$\rho^* \in \left[\rho^*_{TS2}, \rho^*_{TS1}\right]. \tag{64}$$

When the transmitter adopts 2-PPM without using UsIM, the P_{e1} becomes the BER of PPM-SDJD. According to (63), we can obtain the optimal splitting ratio of SDJD is ρ^*_{TS1}.

By performing similar derivations as the TS case, we can obtain the optimal splitting ratio for the PS case as $\rho^* \in [\rho^*_{PS2}, 1]$, where ρ^*_{PS2} is given in (46). Similarly, for PPM-SDJD, the optimal splitting ratio is $\rho^*_{PS1} = 1$.

REFERENCES

[1] W. J. Tomlinson, S. Banou, C. Yu, M. Stojanovic, and K. R. Chowdhury, "Comprehensive survey of galvanic coupling and alternative intra-body communication technologies," *IEEE Commun. Surveys Tuts*, vol. 21, no. 2, pp. 1145–1164, 2nd Quart. 2019.

[2] G. E. Santagati, N. Dave, and T. Melodia, "Design and performance evaluation of an implantable ultrasonic networking platform for the Internet of Medical Things," *IEEE/ACM Trans. Netw.*, vol. 28, no. 1, pp. 29–42, Feb. 2020.

[3] G. E. Santagati, T. Melodia, L. Galluccio, and S. Palazzo, "Ultrasonic networking for E-health applications," *IEEE Wireless Commun.*, vol. 20, no. 4, pp. 74–81, Aug. 2013.

[4] S. E. Trevlakis, A. A. Boulogeorgos, N. D. Chatzidiamantis, and G. K. Karagiannidis, "All-optical cochlear implants," *IEEE Trans. Mol. Biol. Multi-Scale Commun.*, vol. 6, no. 1, pp. 13–24, Jul. 2020.

[5] A. Singer, M. Oelze, and A. Podkowa, "Mbps experimental acoustic through-tissue communications: MEAT-COMMS," in *Proc. IEEE Int. Workshop SPAWC*, Edinburgh, U.K., 2016, pp. 1–4.

[6] U.S. food drug administration (FDA). "Marketing clearance of diagnostic ultrasound systems and transducers." 2019. [Online]. Available: https://www.fda.gov/media/71100/download

[7] G. E. Santagati and T. Melodia, "Experimental evaluation of impulsive ultrasonic intra-body communications for implantable biomedical devices," *IEEE Trans. Mobile Comput.*, vol. 16, no. 2, pp. 367–380, Feb. 2017.

[8] T. Misaridis and J. A. Jensen, "Use of modulated excitation signals in medical ultrasound. Part I: Basic concepts and expected benefits," *IEEE Trans. Ultrason., Ferroelect., Freq. Control*, vol. 52, no. 2, pp. 177–191, Feb. 2005.

[9] G. E. Santagati, T. Melodia, L. Galluccio, and S. Palazzo, "Medium access control and rate adaptation for ultrasonic intrabody sensor networks," *IEEE/ACM Trans. Netw.*, vol. 23, no. 4, pp. 1121–1134, Aug. 2015.

[10] Q. Wang, Q. Guan, B. Ma, and J. Liu, "Direct-sequence ultrasonic wideband technology for intra-body communications," *IEEE Commun. Lett.*, vol. 23, no. 10, pp. 1744–1747, Oct. 2019.

[11] Q. Wang, Q. Guan, J. Cheng, and B. Ma, "Ultrasonic indexed modulation and multiple access for intra-body networks," *IEEE Trans. Commun.*, vol. 69, no. 1, pp. 108–120, Jan. 2021.

[12] W. Liu, X. Zhou, S. Durrani, and P. Popovski, "A novel receiver design with joint coherent and non-coherent processing," *IEEE Trans. Commun.*, vol. 65, no. 8, pp. 3479–3493, Aug. 2017.

[13] Y. Wang, W. Liu, X. Zhou, and G. Liu, "On the performance of splitting receiver with joint coherent and non-coherent processing," *IEEE Trans. Signal Process.*, vol. 68, pp. 917–930, Jan. 2020.

[14] Q. Wang, Q. Guan, J. Cheng, and F. Ji, "A splitting-detection joint-decision receiver for ultrasonic intra-body communications," *IEEE Trans. Commun.*, vol. 69, no. 6, pp. 3586–3597, Jun. 2021.

[15] R. Zhang and C. K. Ho, "MIMO broadcasting for simultaneous wireless information and power transfer," *IEEE Trans. Wireless Commun.*, vol. 12, no. 5, pp. 1989–2001, May 2013.

[16] X. Zhou, R. Zhang, and C. K. Ho, "Wireless information and power transfer: Architecture design and rate-energy tradeoff," *IEEE Trans. Commun.*, vol. 61, no. 11, pp. 4754–4767, Nov. 2013.

[17] Q. Li, M. Wen, E. Basar, and F. Chen, "Index modulated OFDM spread spectrum," *IEEE Trans. Wireless Commun.*, vol. 17, no. 4, pp. 2360–2374, Apr. 2018.

[18] Q. Li, M. Wen, E. Basar, H. V. Poor, and F. Chen, "Spatial modulation-aided cooperative NOMA: Performance analysis and comparative study," *IEEE J. Sel. Topics Signal Process.*, vol. 13, no. 3, pp. 715–728, Jun. 2019.

[19] Q. Wang, Q. Guan, and F. Ji, "A low-complexity splitting receiver for ultrasonic index modulation-based intra-body communications," in *Proc. 30th Biennial Symp. Commun.*, 2022, pp. 101–113.

[20] Z. Guan, G. E. Santagati, and T. Melodia, "Distributed algorithms for joint channel access and rate control in ultrasonic intra-body networks," *IEEE/ACM Trans. Netw.*, vol. 24, no. 5, pp. 3109–3122, Oct. 2016.

[21] M. Z. Win and R. A. Scholtz, "Ultra-wide bandwidth time-hopping spread-spectrum impulse radio for wireless multiple-access communications," *IEEE Trans. Commun.*, vol. 48, no. 4, pp. 679–689, Apr. 2000.

[22] K. Witrisal et al., "Noncoherent ultra-wideband systems," *IEEE Signal Process. Mag.*, vol. 26, no. 4, pp. 48–66, Jul. 2009.

[23] G. Kaddoum, Y. Nijsure, and H. Tran, "Generalized code index modulation technique for high-data-rate communication systems," *IEEE Trans. Veh. Technol.*, vol. 65, no. 9, pp. 7000–7009, Sep. 2016.

[24] A. Papoulis, *Probability, Random Variables, and Stochastic Processes*. New York, NY, USA: McGraw-Hill, 1991.

[25] J. Proakis and M. Salehi, *Digital Communication*, 5th ed. New York, NY, USA: McGraw-Hill, 2008.

[26] T. Cover and J. Thomas, *Elements of Information Theory*. Hoboken, NJ, USA: Wiley, 2006.

[27] M. Wen, X. Cheng, M. Ma, B. Jiao, and H. V. Poor, "On the achievable rate of OFDM with index modulation," *IEEE Trans. Signal Process.*, vol. 64, no. 8, pp. 1919–1932, Apr. 2016.

[28] S. Dolinar, D. Divsalar, J. Hamkins, and F. Pollara, "Capacity of pulse-position modulation (PPM) on Gaussian and Webb channels," Jet Propul. Lab., California Inst. Technol., Pasadena, CA, USA, JPL TMO Progress Rep. 42–142, Apr.-Jun. 2000.

[29] W. C. Lindsey and M. K. Simon, *Telecommunication System Engineering*. Hoboken, NJ, USA: Prentice Hall, 1973.

QIANQIAN WANG (Member, IEEE) received the B.S. degree in electronic information engineering from Nanchang University, Nanchang, China, in 2017, and the Ph.D. degree in information and communication engineering from the South China University of Technology, Guangzhou, China, in 2022. From 2021 to 2022, she was a visiting Ph.D. student with The University of British Columbia, Canada. She is currently an Associate Professor with the College of Computer Science and Engineering, Northwest Normal University, Lanzhou, China, and a Visiting Scholar with Guangdong Provincial Key Laboratory of Short-Range Wireless Detection and Communication, Guangzhou. Her current research interests include ultrasonic intra-body sensor networks and unconventional data communications.

QUANSHENG GUAN (Senior Member, IEEE) received the B.Eng. degree in electronic engineering from the Nanjing University of Post and Telecommunications, China, in 2006, and the Ph.D. degree from the South China University of Technology (SCUT) in 2011.

From 2009 to 2010, he was a visiting Ph.D. student with The University of British Columbia, Canada. From 2012 to 2013, he was a Postdoctoral Researcher with the Chinese University of Hong Kong. He was a Visiting Scholar with the Singapore University of Technology and Design in 2013 and a Visiting Professor with Polytech Nantes, France. He is currently a Full Professor with the School of Electronic and Information Engineering, SCUT. His research interests include wireless communications and networking, underwater acoustic networking, fog/cloud computing, and networked interactions and economics. He is the co-recipient of Best Paper Awards from IEEE ICCC 2014 and IEEE ICNC 2016, and the Best Demo Award from ACM WUWNET 2018. He was a Guest Editor for Mobile Information System, and currently an Associate Editor for IEEE ACCESS and *International Journal of Distributed Sensor Networks*. He has been a TPC member for numerous conferences, and a reviewer for peer-reviewed journals and conferences.

YUANKUN TANG (Graduate Student Member, IEEE) received the B.S. degree in communication engineering from the South China University of Technology, Guangzhou, China, in 2018, where he is currently pursuing the Ph.D. degree in information and communication engineering. He was a visiting student with Yonsei University, Seoul, South Korea, in August 2019. He was with the University of Southampton as a visiting student from November 2021 to November 2022. His main research interests include molecular communications and wireless communications. He received the Best Student Paper Award from the IEEE International Conference on Computer and Communication Systems in 2023.

JULIAN CHENG (Fellow, IEEE) received the B.Eng. degree (Hons.) in electrical engineering from the University of Victoria, Victoria, BC, Canada, in 1995, the M.Sc. (Eng.) degree in mathematics and engineering from Queens University, Kingston, ON, Canada, in 1997, and the Ph.D. degree in electrical engineering from the University of Alberta, Edmonton, AB, Canada, in 2003. He was with Bell Northern Research and NORTEL Networks. He is currently a Full Professor with the School of Engineering, Faculty of Applied Science, The University of British Columbia, Kelowna, BC, Canada. His research interests include machine learning and deep learning for wireless communications, wireless optical technology, and quantum communications. He was the Co-Chair of the 12th Canadian Workshop on Information Theory in 2011, the 28th Biennial Symposium on Communications in 2016, and the Sixth EAI International Conference on Game Theory for Networks in 2016. He was the General Co-Chair of the 2021 IEEE Communication Theory Workshop. He is the Chair of the Radio Communications Technical Committee of the IEEE Communications Society. He served as the President for the Canadian Society of Information Theory from 2017 to 2021. He was a past Associate Editor of the IEEE TRANSACTIONS ON COMMUNICATIONS, the IEEE TRANSACTIONS ON WIRELESS COMMUNICATIONS, the IEEE COMMUNICATIONS LETTERS, and IEEE ACCESS, as well as an Area Editor of the IEEE TRANSACTIONS ON COMMUNICATIONS. He served as a Guest Editor for a Special Issue of the IEEE JOURNAL ON SELECTED AREAS IN COMMUNICATIONS on Optical Wireless Communications. He is a registered Professional Engineer in BC, Canada.

FEI JI (Member, IEEE) received the B.S. degree in applied electronic technologies from Northwestern Polytechnical University, Xi'an, China, in 1992, and the M.S. degree in bioelectronics and the Ph.D. degree in circuits and systems from the South China University of Technology, Guangzhou, China, in 1995 and 1998, respectively. She was a Visiting Scholar with the University of Waterloo, Waterloo, ON, Canada, from June 2009 to June 2010. She was a Research Assistant with the City University of Hong Kong, Hong Kong, from March 2001 to July 2002 and a Senior Research Associate from January 2005 to March 2005. She is currently a Professor with the School of Electronic and Information Engineering, South China University of Technology. Her research interests include wireless communication systems and networking. She was the Registration Chair and a Technical Program Committee Member of the IEEE 2008 International Conference on Communication Systems.

XIANGDONG JIA (Member, IEEE) received the M.S. degree in communication and information engineering from Anhui University, Hefei, China, in 2007, and the Ph.D. degree in communication and information engineering from the Nanjing University of Posts and Telecommunications, Nanjing, China, in 2011. He is currently a Professor with the College of Computer Science and Engineering, Northwest Normal University, Lanzhou, China. His research interests include wireless communications, next generation networks, relay, cache, cooperative communications, cognitive radio, massive MIMO, and age of information.